Astigmatic electron diffraction imaging: a novel mode for structure determination

W. McBride, N. L. O'Leary, K. A. Nugent and L. J. Allen*

School of Physics, University of Melbourne, Victoria 3010, Australia. Correspondence e-mail: lja@physics.unimelb.edu.au

In a conventional transmission electron microscope, stigmators are used to correct for the effects of axial astigmatism in the diffraction lens. It seems feasible that these same stigmators could also be used to form a series of 'astigmatic' diffraction patterns. It is shown how this series of diffraction patterns could then be used to perform exit-surface wavefunction reconstruction. This has the advantage that the diffraction patterns are not resolution limited by the objective aperture as are images when performing exit-surface wavefunction reconstruction from a focal series. A scheme for carrying out phase reconstruction from a series of astigmatic diffraction patterns in an electron microscope is presented.

1. Introduction

Diffraction is a phenomenon that has proven to be remarkably useful for investigating the structure of matter. A beam of radiation, comprised of waves propagating in free space and usually formed by X-rays, neutrons or electrons, diffracts through an object and a measurement of the intensity in the far field (the diffraction pattern) is made. From the distribution of the intensity in the diffraction pattern, a wealth of information about the structure of the object can be deduced. However, the structure cannot be uniquely determined unless the phase of the wavefield corresponding to the diffraction pattern can be determined. This is an example of a 'phase problem'.

The crystallographic phase problem has a long history (Millane, 1990). Here we consider an approach not restricted to crystals. In this context, numerous approaches to phase reconstruction have been developed in different contexts (Gerchberg & Saxton, 1972; Saxton, 1978; Fienup, 1982; Teague, 1983; Fienup, 1987; Paganin & Nugent, 1998; Allen & Oxley, 2001; Miao, Amonette et al., 2003; Allen, McBride, O'Leary & Oxley, 2004). Often these approaches utilize a priori information pertaining to the object or the beam of radiation in combination with measurements of the intensity of the wavefield taken in the near field (Saxton, 1994) and/or the far field (Miao & Sayre, 2000). The dependence on a priori information places restrictions on the generality of any given method. For example, to execute a successful phase reconstruction some methods require a priori information that the object being investigated is a 'weak-phase' object (Misell & Greenaway, 1974), or that the object can be isolated within the beam of radiation (Robinson et al., 2001; Zuo et al., 2003).

Various phase-reconstruction schemes have exploited the fact that both images and diffraction patterns can be used to effect reconstruction (Misell, 1973; Chapman, 1975a,b).

However, in certain situations, only a diffraction pattern of the object can be formed and, when an image is obtainable, the resolution is usually lower than that of the corresponding diffraction pattern. Hence the current interest in 'diffraction imaging' (Spence et al., 2001; Weierstall et al., 2002; Miao, Ishikawa et al., 2003). Realizing this goal for a single diffraction pattern is not straightforward; some reasonably strong restrictions have to be placed on the type of object being investigated before phase reconstruction can be achieved. Consequently, several authors have investigated the possibility of modifying the object or the incident beam to form two or more diffraction patterns, which can then be used to perform phase reconstruction (Walker, 1981; Kim & Hayes, 1990).

The notion of using several diffraction patterns to perform phase reconstruction, with the aim of extending the range of objects to which phase reconstruction can be applied, has recently been investigated by Nugent et al. (2003). In that work, the authors propose modifying the phase of the incident beam to produce several different diffraction patterns from the same object. Beams with cylindrical phase curvature are incident upon the sample and hence the diffraction patterns produced are referred to as 'astigmatic'. They also show that, for a weak phase object, when the phase modification of the incident beam is very small, a unique solution for the phase reconstruction exists. 'We are therefore able to conclude that a measurement of the far-field diffraction pattern combined with far-field diffraction patterns obtained with orthogonal cylindrically curved waves is sufficient to uniquely determine the phase of the diffraction pattern' (Nugent et al., 2003).

In this paper, we present a phase-reconstruction method based on astigmatic diffraction in a conventional transmission electron microscope (CTEM). The method is founded upon the electron-optical configuration used to observe a diffraction pattern in a CTEM in which a post-specimen lens, the 'diffraction lens', images the back focal plane of the objective

lens, hence an astigmatic diffraction lens will form an astigmatic diffraction pattern. Using this optical arrangement to collect data for phase reconstruction has several advantages: the resolution of the data is not limited by the use of the objective aperture and, as the phase modifications are made post specimen, the phase can be reconstructed for specimens where multiple scattering has occurred. We investigate the orientation and strength of the astigmatism needed to effect phase retrieval and the accuracy with which it needs to be known.

2. Theory

2.1. Astigmatic diffraction

Denote the wavefunction imaged by the diffraction lens in a CTEM as $\psi(\mathbf{r})$. The wavefunction in the back focal plane of the diffraction lens is given by

$$\psi(\mathbf{p}) = \mathcal{F}[T_d(\mathbf{r}) \otimes \psi(\mathbf{r})] = T_d(\mathbf{p})\mathcal{F}[\psi(\mathbf{r})], \qquad (1)$$

where $\mathbf{p}$ is the momentum-space vector conjugate to $\mathbf{r}$ and

$$T_d(\mathbf{p}) = A_d(\mathbf{p}) \exp[-i\chi_d(\mathbf{p})] \qquad (2)$$

is the transfer function of the diffraction lens. The effective aperture function $A_d(\mathbf{p})$ is unity and

$$\chi_d(\mathbf{p}) = \pi\lambda\Delta f p^2 + 0.5\pi\lambda^3 C_s p^4 + \pi\lambda C_a p^2 \cos[2(\phi - \phi_a)], \qquad (3)$$

where λ is the electron wavelength, Δf is defocus, C_s is the coefficient of spherical aberration and C_a is the coefficient of astigmatism. The angle ϕ is the polar angle of the momentum-space vector $\mathbf{p}$ and ϕ_a designates the orientation of the astigmatism. This notation assumes that Δf is positive for overfocus.

For an object of extent ~ 100 Å and incident radiation of 300 keV, the maximum transverse momentum component of the wave in the diffraction plane $p_{max} \approx 1 \times 10^{-4}$ Å. This means that the spherical aberration term in equation (3) can be ignored. Although astigmatism in the diffraction lens is generally corrected using stigmators (Champness, 2001), its presence (usually considered to be a nuisance) makes it possible to form astigmatic diffraction patterns. Axial astigmatism as described in equation (3) models the plane of least confusion. In practice, when adding astigmatism systematically to a diffraction pattern, one would observe either the sagittal or the meridional focus plane, depending on how the astigmatism was applied. To model this situation, we choose to observe the meridional focus plane and do this by overfocusing the diffraction lens such that $\Delta f = C_a$. Including these modifications in equation (3) gives

$$\chi_d(\mathbf{p}) = \pi\lambda C_a p^2 \{1 + \cos[2(\phi - \phi_a)]\}. \qquad (4)$$

By operating a CTEM in diffraction mode and systematically varying the astigmatism in the diffraction lens, we can thus produce a series of 'astigmatic' diffraction patterns. These patterns can then be used to perform phase reconstruction.

2.2. Phase-reconstruction method

Fig. 1 shows the scheme used to perform phase reconstruction. Its design is similar in spirit to several other methods that have been developed (Gerchberg & Saxton, 1972; Misell & Greenaway, 1974; Saxton, 1978; Allen & Oxley, 2001; Nugent et al., 2003; Allen, McBride, O'Leary & Oxley, 2004), although most of these schemes have been applied to a focal series of images. To demonstrate our approach, three diffraction patterns are shown in Fig. 1. In practice, more diffraction patterns can be employed.

1. An initial estimate $\xi_{n=0}(\mathbf{p})$ of the wavefunction $\xi(\mathbf{p}) = \mathcal{F}[\psi(\mathbf{r})]$ in the back focal plane of the diffraction lens is made. Typically, we set $\xi_{n=0}(\mathbf{p}) = 1$, which is a plane wave of unit amplitude and zero phase.

2. $\xi_{n=0}(\mathbf{p})$ is multiplied by the phase factor $\exp[-i\chi_{d_1}(\mathbf{p})]$ describing the applied astigmatism.

3. $\xi_{n=0}(\mathbf{p})\exp[-i\chi_{d_1}(\mathbf{p})]$ is Fourier transformed and its amplitude is corrected by replacement with the square root of the intensity of diffraction pattern 1.

4. The wavefunction is inverse Fourier transformed and the phase factor $\exp[-i\chi_{d_1}(\mathbf{p})]$ divided out.

5. Steps 2–4 are repeated for the phase factors and diffraction patterns 2 and 3.

6. At this point, an improved wavefunction estimate $\xi_{n=n+1}(\mathbf{p})$ has been obtained. The convergence of the method is checked and iteration continues if the convergence criterion is not satisfied. Otherwise the scheme terminates.

There are alternative ways to construct the scheme shown in Fig. 1. In other work (Allen, McBride & Oxley, 2004), we have shown that a 'global' approach can be more robust in the presence of experimental uncertainties.
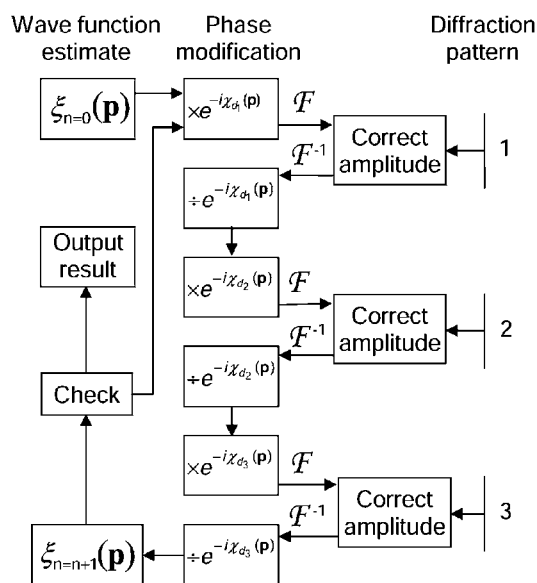

Figure 1
Schematic diagram depicting the astigmatic diffraction phase reconstruction method for three diffraction patterns. The symbol $\mathcal{F}$ denotes a Fourier transform and $\mathcal{F}^{-1}$ an inverse Fourier transform.

3. Results and discussion

To test the utility of this method, an exit-surface wavefunction (ESWF) obtained from a focal series of atomic resolution images of β-Si_3N_4 with electrons incident in the [0001] direction (Ziegler *et al.*, 2002; Allen, McBride, O'Leary & Oxley, 2004) was used as a test object. Fig. 2(*a*) shows the image and Fig. 2(*b*) shows the phase of this ESWF. The image and phase map are 512×512 pixels and each pixel is 0.2×0.2 Å. Hence the dimensions of the object are 102.4×102.4 Å.

Using the ESWF shown in Fig. 2, C_a was varied systematically to simulate multiple series of astigmatic diffraction patterns. For each value of C_a, seven diffraction patterns were
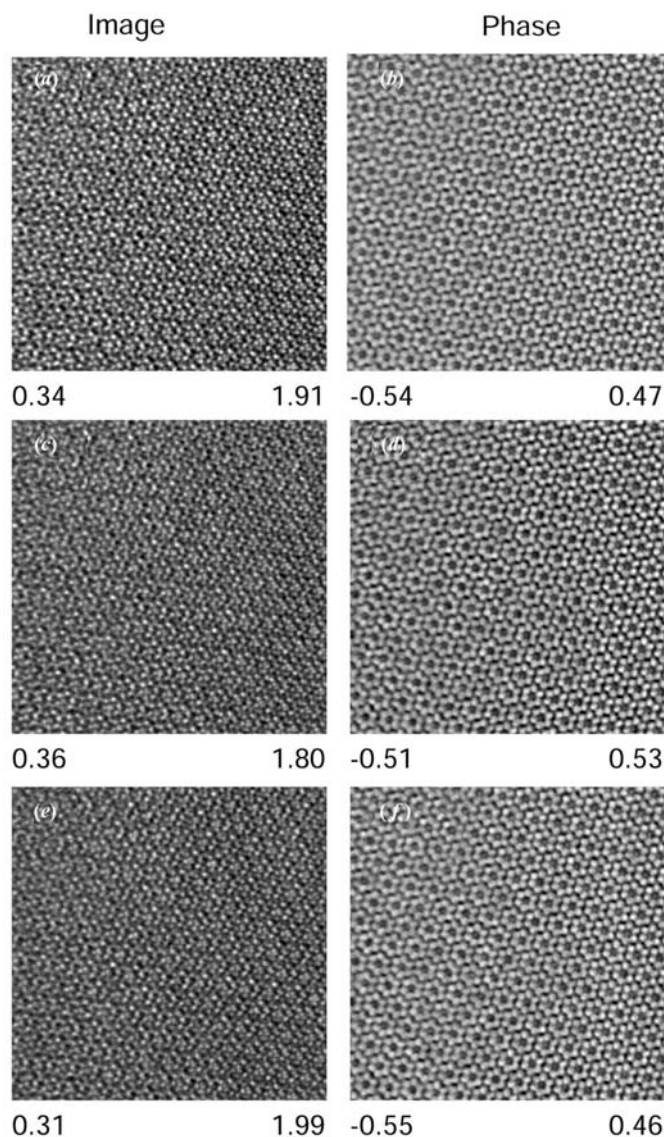
simulated. One diffraction pattern in each series had no astigmatism applied to it (for purposes of comparison). The remaining diffraction patterns were obtained by varying the axis of astigmatism, *i.e.* ϕ_a took the values $\pi/6$, $\pi/3$, $\pi/2$, $2\pi/3$, $5\pi/6$ and π. For all simulations, the value of $f = 2$ mm, which is typical for a CTEM, and $\lambda = 0.0197$ Å were used. Such a

Image   Phase

Figure 2
(*a*) An exit-surface image and (*b*) phase of β-Si_3N_4 viewed along the [0001] zone axis, each image is 512×512 pixels and each pixel is 0.2×0.2 Å. The intensity and phase ranges are displayed at the foot of each image. (*c*) The image and (*d*) phase reconstructed from the series of astigmatic diffraction patterns shown in Fig. 3. (*e*) The image and (*f*) phase reconstructed from the series of astigmatic diffraction patterns shown in Fig. 3 with noise added to each diffraction pattern as described in the text.
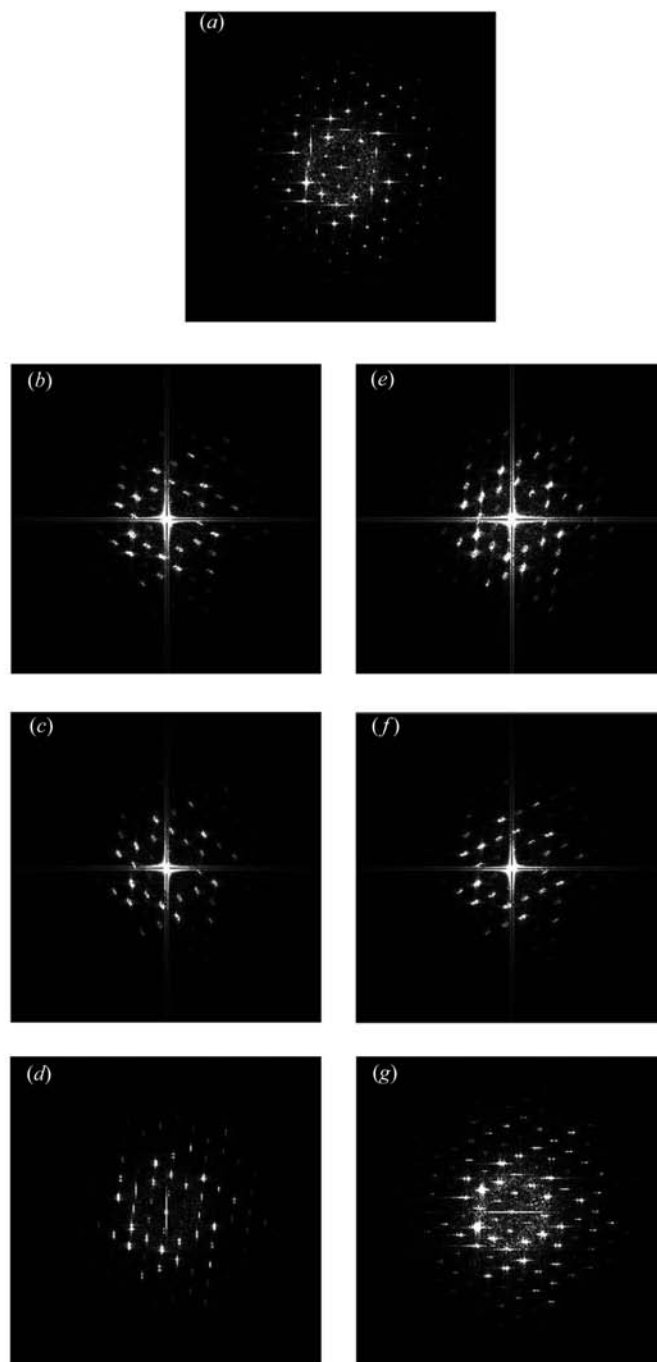
Figure 3
Diffraction patterns formed from the ESWF corresponding to Figs. 2(*a*) and 2(*b*) and using equation (4). (*a*) $C_a = 0$ and $\phi_a = 0$. (*b*) $C_a = 100$ mm and $\phi_a = \pi/6$. (*c*) $C_a = 100$ mm and $\phi_a = \pi/3$. (*d*) $C_a = 100$ mm and $\phi_a = \pi/2$. (*e*) $C_a = 100$ mm and $\phi_a = 2\pi/3$. (*f*) $C_a = 100$ mm and $\phi_a = 5\pi/6$. (*g*) $C_a = 100$ mm and $\phi_a = \pi$. The diffraction patterns have the same scale but their contrast has been adjusted to highlight the less intense diffraction spots.

series of diffraction patterns for $C_a = 100$ mm is shown in Fig. 3.

Estimates for the value of C_a needed to effect an accurate phase reconstruction were deduced by observing the results of the phase reconstructions obtained from each separate astigmatic diffraction series. For the various astigmatic diffraction series simulated from the ESWF shown in Fig. 3, accurate phase reconstructions were obtained for $C_a \geq 100$ mm, although reasonable phase reconstructions with C_a values as low as 50 mm were still possible. Fig. 2(c) shows the image and Fig. 2(d) shows the phase reconstructed from the simulated astigmatic diffraction series shown in Fig. 3 ($C_a = 100$ mm).

To further test this method, simulations were performed in which noise was added to each diffraction pattern in the series of astigmatic diffraction patterns shown in Fig. 3. This was done by adding 0.01% noise to the largest pixel value in the diffraction pattern, with correspondingly larger amounts of noise on less intense pixels where the number of counts is lower. The statistical error for each intensity value was calculated using a random deviate drawn from a Poisson distribution (Press *et al.*, 1986). Fig. 2(e) shows the image and Fig. 2(f) shows the phase reconstructed from these diffraction patterns and demonstrates the robustness of this approach in the presence of noise. Noise occurs differently in each diffraction pattern so that an overdetermined wavefunction reconstruction, using several patterns, is robust in the presence of quite high levels of noise. Numerical tests also show that, for similar reasons, with inaccuracies in C_a of up to 5% and uncertainties in the axis of astigmatism ϕ_a of up to 0.05 rad, excellent reconstructions are still obtained. Using a set of high-resolution diffraction patterns is advantageous relative to methods based on low-resolution images or the hybrid approach of phase extension, where a single high-resolution diffraction pattern and a single low-resolution image are used, see for example Fan *et al.* (1985).

For experimental conditions in which p_{max} is increased, equation (4) suggests that lower values of C_a will suffice for robust ESWF reconstruction. We tested this by assuming that our test object was 16 times larger. This was confirmed for the case analogous to the diffraction patterns shown in Fig. 3, a value of $C_a = 5$ mm now allowing accurate ESWF reconstruction.

4. Conclusions

A method for performing phase reconstruction from a series of astigmatic diffraction patterns in a CTEM has been presented. Although our test case was *a priori* aperture limited owing to its construction from an ESWF based on actual high-resolution TEM images, in practice it will have the advantage that ESWF reconstruction is possible without the resolution limiting effect of the objective aperture. The ESWF for strongly multiply scattering objects can be reconstructed.

References

Allen, L. J., McBride, W., O'Leary, N. L. & Oxley, M. P. (2004). *Ultramicroscopy*, **100**, 91–104.
Allen, L. J., McBride, W. & Oxley, M. P. (2004). *Opt. Commun.* **233**, 77–82.
Allen, L. J. & Oxley, M. P. (2001). *Opt. Commun.* **199**, 65–75.
Champness, P. E. (2001). *Electron Diffraction in the Transmission Electron Microscope.* Oxford: BIOS Scientific Publishers.
Chapman, J. N. (1975a). *Philos. Mag.* **32**, 527–540.
Chapman, J. N. (1975b). *Philos. Mag.* **32**, 541–552.
Fan, H.-F., Zhong, Z.-Y., Zheng, C.-D. & Li, F.-H. (1985). *Acta Cryst.* A**41**, 163–165.
Fienup, J. R. (1982). *Appl. Opt.* **21**, 2758–2769.
Fienup, J. R. (1987). *J. Opt. Soc. Am.* A**4**, 118–123.
Gerchberg, R. W. & Saxton, W. O. (1972). *Optik (Stuttgart)*, **35**, 237–246.
Kim, W. & Hayes, M. H. (1990). *J. Opt. Soc. Am.* A**7**, 441–449.
Miao, J., Amonette, J. E., Nishino, Y., Ishikawa, T. & Hodgson, K. O. (2003). *Phys. Rev. B*, **68**, 012201.
Miao, J., Ishikawa, T., Anderson, E. H. & Hodgson, K. O. (2003). *Phys. Rev. B*, **67**, 174104.
Miao, J. & Sayre, D. (2000). *Acta Cryst.* A**56**, 596–605.
Millane, R. P. (1990). *J. Opt. Soc. Am.* A**7**, 394–411.
Misell, D. L. (1973). *J. Phys. D: Appl. Phys.* **6**, L6–L9.
Misell, D. L. & Greenaway, A. H. (1974). *J. Phys. D: Appl. Phys.* **7**, 832–855.
Nugent, K. A., Peele, A. G., Chapman, H. N. & Mancuso, A. P. (2003). *Phys. Rev. Lett.* **91**, 203902.
Paganin, D. & Nugent, K. A. (1998). *Phys. Rev. Lett.* **80**, 2586–2589.
Press, W. H., Teukolsky, S. A., Vetterling, W. T. & Flannery, B. P. (1986). *Numerical Recipes in Fortran: the Art of Scientific Computing*, 2nd ed. Cambridge University Press.
Robinson, I. K., Vartanyants, I. A., Williams, G. J., Pfeifer, M. A. & Pitney, J. A. (2001). *Phys. Rev. Lett.* **87**, 195505.
Saxton, W. O. (1978). *Computer Techniques for Image Processing in Electron Microscopy.* New York: Academic Press.
Saxton, W. O. (1994). *Ultramicroscopy*, **55**, 171–181.
Spence, J. C. H., Howells, M., Marks, L. D. & Miao, J. (2001). *Ultramicroscopy*, **90**, 1–6.
Teague, M. R. (1983). *J. Opt. Soc. Am.* **73**, 1434–1441.
Walker, J. G. (1981). *Opt. Acta*, **28**, 735–738.
Weierstall, U., Chen, Q., Spence, J. C. H., Howells, M. R., Isaacson, M. & Panepucci, R. R. (2002). *Ultramicroscopy*, **90**, 171–195.
Ziegler, A., Kisielowski, C. & Ritchie, R. O. (2002). *Acta Mater.* **50**, 565–574.
Zuo, J. M., Vartanyants, I. A., Gao, M., Zhang, R. & Nagahara, L. A. (2003). *Science*, **300**, 1419–1421.